Perturbation of Polyamine Catabolism Can Strongly Affect Root Development and Xylem Differentiation[1][W]

Alessandra Tisi, Rodolfo Federico, Sandra Moreno, Sergio Lucretti, Panagiotis N. Moschou, Kalliopi A. Roubelakis-Angelakis, Riccardo Angelini, and Alessandra Cona*

Department of Biology, University Roma Tre, 00146 Rome, Italy (A.T., R.F., S.M., R.A., A.C.); ENEA Casaccia Research Center, BIOTEC GEN, 00123 Rome, Italy (S.L.); and Department of Biology, University of Crete, 71409 Heraklion, Greece (P.N.M., K.A.R.-A.)

Spermidine (Spd) treatment inhibited root cell elongation, promoted deposition of phenolics in cell walls of rhizodermis, xylem elements, and vascular parenchyma, and resulted in a higher number of cells resting in G_1 and G_2 phases in the maize (*Zea mays*) primary root apex. Furthermore, Spd treatment induced nuclear condensation and DNA fragmentation as well as precocious differentiation and cell death in both early metaxylem and late metaxylem precursors. Treatment with either *N*-prenylagmatine, a selective inhibitor of polyamine oxidase (PAO) enzyme activity, or *N*,*N*[1]-dimethylthiourea, a hydrogen peroxide (H_2O_2) scavenger, reverted Spd-induced autofluorescence intensification, DNA fragmentation, inhibition of root cell elongation, as well as reduction of percentage of nuclei in S phase. Transmission electron microscopy showed that *N*-prenylagmatine inhibited the differentiation of the secondary wall of early and late metaxylem elements, and xylem parenchymal cells. Moreover, although root growth and xylem differentiation in antisense *PAO* tobacco (*Nicotiana tabacum*) plants were unaltered, overexpression of maize *PAO* (S-*ZmPAO*) as well as down-regulation of the gene encoding *S*-adenosyl-L-methionine decarboxylase via RNAi in tobacco plants promoted vascular cell differentiation and induced programmed cell death in root cap cells. Furthermore, following Spd treatment in maize and *ZmPAO* overexpression in tobacco, the in vivo H_2O_2 production was enhanced in xylem tissues. Overall, our results suggest that, after Spd supply or PAO overexpression, H_2O_2 derived from polyamine catabolism behaves as a signal for secondary wall deposition and for induction of developmental programmed cell death.

Polyamines (PAs) are ubiquitous, low-molecular mass aliphatic polycations. These compounds include the diamine putrescine (Put), the triamine spermidine (Spd), and the tetraamine spermine (Spm), as well as the less common 1,3-diaminopropane (DAP), cadaverine, norspermidine, norspermine, and thermospermine. It has been suggested that PAs participate in cell growth and differentiation, by regulating cell cycle progression and physicochemical properties of membranes, as well as by influencing the stabilization and protection of nucleic acid and protein structure (Cohen, 1998). Their essential role in cell growth and differentiation (Torrigiani et al., 1987; Wallace et al., 2003; Kusano et al., 2008) has been strongly supported by the observation that the loss of function of genes involved in PA biosynthesis results in early embryonic lethality in mouse (Wang et al., 2004), and in lethal defects in embryonic development in Arabidopsis (*Arabidopsis thaliana*; Imai et al., 2004; Urano et al., 2005; Ge et al., 2006). Consistent with the role of PAs as positive regulators of cell growth, these compounds protect cells from apoptosis and their overproduction has been linked to cell overproliferation and malignant development in animal cells (Wallace et al., 2003). On the other hand, either the increase or the decrease of physiological levels of PAs, induce the execution of the programmed cell death (PCD) syndrome (Seiler and Raul, 2005) either by caspase activation (Stefanelli et al., 1998) or cytochrome *c* release from mitocondria (Stefanelli et al., 2000), revealing PAs as bivalent regulators of cellular functions.

In plants, it has been suggested that PAs play important roles in diverse developmental processes, including morphogenesis, growth, differentiation, and senescence. Moreover, they are implicated in defense responses to various biotic and abiotic stresses (Bouchereau et al., 1999; Walters, 2003; Kusano et al., 2007; Cuevas et al., 2008) and participate in signaling pathways by regulation of cation channel activities (Kusano et al., 2008) such as during stomatal closure (Liu et al., 2000) and salt stress response (Zhao et al., 2007). As concerns root development, it has been reported that exogenously supplied Spd affects cell elongation and shape as well as the mitotic index in maize (*Zea mays*) primary roots (de Agazio et al., 1995). The involvement of PAs in vascular development (Vera-Sirera et al., 2010) has been recently highlighted by investigation of the Arabidopsis dwarf mutant *bud2*

[1] This work was supported by the Italian Ministry for University and Research (Progetti di Ricerca di Interesse Nazionale 2007, project contract no. 2007K7KY8Y_001 to R.A.) and University Roma Tre, Italy.

* Corresponding author; e-mail cona@uniroma3.it.

The author responsible for distribution of materials integral to the findings presented in this article in accordance with the policy described in the Instructions for Authors (www.plantphysiol.org) is: Alessandra Cona (cona@uniroma3.it).

[W] The online version of this article contains Web-only data.

www.plantphysiol.org/cgi/doi/10.1104/pp.111.173153

(the loss-of-function mutant of an *S*-adenosyl-Met decarboxylase), impaired in PA biosynthesis and homeostasis and displaying enlarged vascular systems in inflorescences, roots, and petioles (Ge et al., 2006). In addition, the importance of PAs in xylem differentiation and cell death has been confirmed by studies of the Arabidopsis mutant of *ACAULIS5* (*acl5*), encoding a thermospermine synthase specifically expressed in the xylem tissues at a precise developmental stage (Knott et al., 2007). This *acl5* mutant shows severely reduced secondary growth of the vascular tissue, dramatically altered morphology of the vessel element, and total lack of xylem fibers (Clay and Nelson, 2005). It has been hypothesized that under physiological conditions, ACL5 prevents premature death of the developing vessel elements to allow complete expansion and secondary cell wall patterning (Muñiz et al., 2008).

PAs are catabolized by two classes of amine oxidases, the copper-containing amine oxidases (CuAOs) and the FAD-dependent amine oxidases (PAOs). CuAOs oxidize Put at the primary amino group producing 4-aminobutyraldehyde (ABAL), hydrogen peroxide (H_2O_2), and ammonia (Medda et al., 2009). PAOs catalyze the oxidation of Spm, Spd, and/or their acetylated derivatives at the secondary amino group (Cona et al., 2006; Angelini et al., 2010). The chemical nature of PAO reaction products depends on the enzyme source and reflects the mode of substrate oxidation. In monocotyledons, PAOs oxidize the carbon at the endo-side of the N^4-nitrogen of Spd and Spm, producing ABAL and *N*-(3-aminopropyl)-ABAL, respectively, in addition to DAP and H_2O_2 (Cona et al., 2006; Angelini et al., 2010). In Arabidopsis, PAOs, namely AtPAO1 (Tavladoraki et al., 2006), AtPAO2 (Fincato et al., 2011), AtPAO3 (Moschou et al., 2008c), and AtPAO4 (Kamada-Nobusada et al., 2008), oxidize the carbon at the exo-side of the N^4-nitrogen of Spd and Spm, giving rise to an interconversion catabolism, with the production of Spd from Spm and Put from Spd, in addition to 3-aminopropionaldehyde and H_2O_2. Thus, H_2O_2 is the only shared compound in all the amine oxidase-catalyzed reactions.

Maize PAO (ZmPAO), the best plant PAO characterized so far, is a 53-kD monomeric glycoprotein, containing one FAD molecule and localizing at the apoplast in mature tissues (Cona et al., 2005, 2006). Indeed, using ultrastructural and immunocytochemical techniques, it has been previously reported that ZmPAO protein is localized in both the cytoplasm and cell wall of developing tracheary elements and in the endodermis of maize primary roots, with a progressive increase of cell wall immunolabeling as the tissues mature (Cona et al., 2005). Until now, three ZmPAO-encoding genes (*ZmPAO1*, *ZmPAO2*, *ZmPAO3*) have been identified that show a conserved organization resulting in identical amino acid sequences except for the substitution of one amino acid in *ZmPAO3* (Cona et al., 2006).

CuAOs and PAOs do not only contribute to important physiological processes through the regulation of cellular PA levels, but do so also through their reaction products: aminoaldehydes, DAP and, markedly, H_2O_2 (Bouchereau et al., 1999; Walters, 2003; Cona et al., 2006; Angelini et al., 2010). In Arabidopsis, intracellular Spd-derived H_2O_2 triggers the opening of the hyperpolarization-activated Ca^{2+}-permeable channels in pollen, thus regulating pollen tube growth (Wu et al., 2010). In tobacco (*Nicotiana tabacum*), H_2O_2 derived from apoplastic PA catabolism is a key molecule in PCD signaling during the cryptogein-induced hypersensitive response (HR; Yoda et al., 2006) as well as in the induction of HR marker genes by mitochondrial dysfunction and activation of mitogen-activated protein kinases (Takahashi et al., 2003; Kusano et al., 2007; Moschou et al., 2009). Moreover, it has been recently demonstrated that salinity stress induces the exodus of Spd into the apoplast, resulting in the induction of a PAO-mediated H_2O_2 burst leading to either tolerance responses or PCD, depending on the levels of intracellular PAs (Moschou et al., 2008b).

The abundant expression of plant CuAOs and ZmPAO in tissues undergoing lignification or extensive cell wall-stiffening events, such as vascular tissues, epidermis, and wound periderm, suggests that these enzymes influence plant growth and development as well as taking part in defense responses by affecting cell wall strengthening and rigidity, through H_2O_2 production (Cona et al., 2005, 2006; Paschalidis and Roubelakis-Angelakis, 2005; Angelini et al., 2008). Importantly, an additional role for CuAOs and PAOs in PCD associated with developmental differentiation, has been proposed (Møller and McPherson, 1998; Cona et al., 2005). Indeed, the presence of PAO (Cona et al., 2005; this work) and CuAO (Møller and McPherson, 1998) proteins in developing root tracheary elements and sloughed root cap cells of maize and Arabidopsis seedlings, respectively, suggests their potential involvement, as H_2O_2-delivering sources, in PCD of both cell types. Thus it is evident that both PA anabolism and catabolism through either cell autonomous and nonautonomous pathways may mediate physiological events associated with PA-induced regulation of growth and development as well as induction of PCD involved in tissue differentiation or defense responses.

In this work, we focused on the role exerted by PAO in root growth and development, and especially in vascular tissue differentiation, by means of both pharmacological and genetic approaches. In particular, we studied PAO expression, by a combined histochemical and immunocytochemical approach, in differentiating maize root tissues, focusing on those tissues undergoing developmental PCD, to achieve full maturity. We also examined the effect of H_2O_2 derived from PAO-mediated catabolism of Spd, on root growth and cell elongation, cell cycle phase distributions, nuclear condensation, and DNA fragmentation. Moreover we investigated the consequences of PAO-mediated H_2O_2 overproduction on early differentiation of metaxylem and protoxylem precursors, to address the issue of the

possible involvement of PAO activity in the PCD of xylem tissues. Finally the effect of the perturbation of PA metabolism on root xylem differentiation was investigated by genetic means, with the aim of discerning the specific contribution of altered PAs on H_2O_2 levels.

Overall, our data suggest that H_2O_2 derived from PA catabolism strongly affects root development and xylem differentiation by inducing differentiation of secondary wall and precocious cell death in xylem precursors of Spd-treated maize primary root as well as by inducing early differentiation of vascular tissues and increased cell death in root cap cells of tobacco root apices from transgenic plants overexpressing *ZmPAO*.

RESULTS

Cell- and Tissue-Specific Expression of PAO in Maize Primary Roots

To investigate the role of ZmPAO in root development, we applied a light-microscope-based histochemical assay, to visualize PAO enzymatic activity on transversal sections at increasing distances from the root cap, up to 1,000 μm from the apical meristem (Fig. 1, A–F), as well as on longitudinal sections of meristematic and differentiating zones (Fig. 1, G and H) of the maize primary root, by 3,3′-diaminobenzidine (DAB) staining, enhanced (Fig. 1, A–F) or not (Fig. 1, G and H) by $CoCl_2$. As shown in Figure 1, B, C, and G, PAO activity was detected in sloughed root cap cells, but not in the columella (Fig. 1A). Concomitant with initial root tissue differentiation, we observed a progressive increase of PAO activity in xylem parenchyma as well as in early metaxylem (EMX) and late metaxylem (LMX) precursors, while PAO enzymatic activity appeared very low in the rhizodermis at the same developmental stage (Fig. 1, C–H). In particular, PAO activity appeared in the procambium (Fig. 1B), greatly increasing as stelar tissues mature up to 1,000 μm from the apical meristem (Fig. 1, B–F). LMX precursors appeared earlier (approximately at 40 μm from the apical meristem, Fig. 1C) than EMX (approximately at 100 μm from the apical meristem, Fig. 1D) in agreement with McCully (1995). As shown in Figure 1H, in the more mature region of the root, where the xylem was well differentiated, high PAO enzymatic activity was evident in the vascular cylinder. Light microscopic, silver-enhanced immunogold labeling revealed that ZmPAO protein accumulated prevalently in the cytoplasm of xylem precursors, xylem parenchyma, and rhizodermis at approximately 1,000 μm from the apical meristem (Fig. 1, I–K). The accumulation of apparently inactive ZmPAO protein in young rhizodermal cells may be related to the necessity of a high extension rate, and thus low H_2O_2 level in the cell wall (Cona et al., 2005), at this developmental stage and to the requirement of H_2O_2 production in the successive wall stiffening events during the maturation phase.

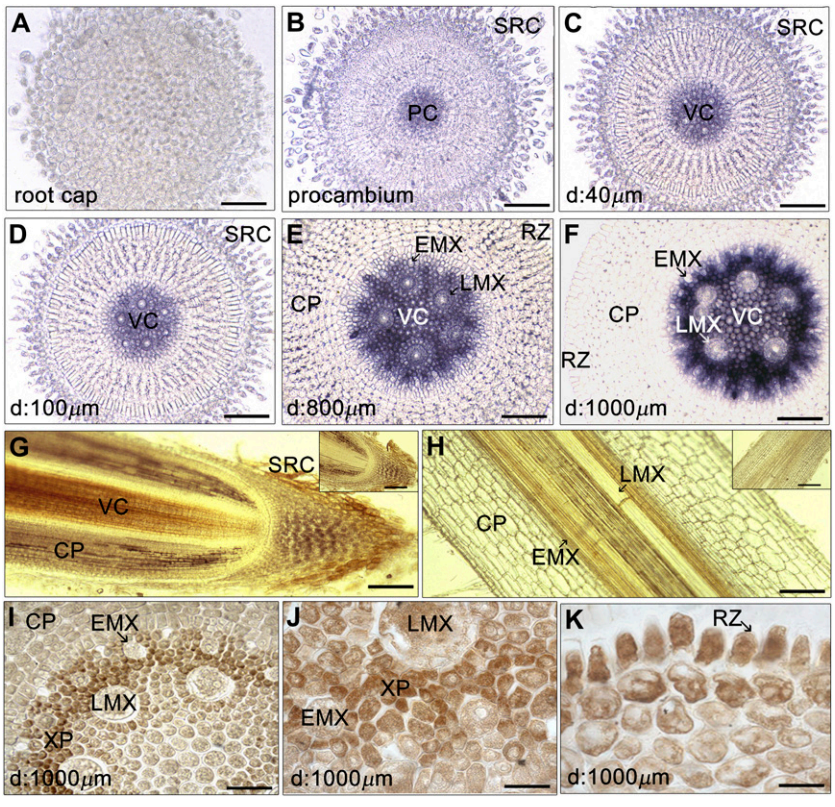

Figure 1. ZmPAO expression in longitudinal and cross sections from maize primary root at different distances from the apical meristem. A to H, Histochemical visualization under light microscope of ZmPAO enzyme activity in agar-embedded vibratome-cut sections. H_2O_2 accumulation, upon Spd addition, was visualized by DAB staining in either cross sections at increasing distances from the root cap up to 1,000 μm from the apical meristem (A–F), or longitudinal sections of both root apex and region of maturation (G and H, respectively). In some sections DAB staining was enhanced by $CoCl_2$ treatment (A–F). Insets illustrate longitudinal control sections without Spd supply. I to K, ZmPAO light microscopic immunolocalization revealed by silver-enhanced immuno-gold staining on paraffin-embedded cross sections at approximately 1,000 μm from the apical meristem. D, Distance from the apical meristem. CP, Cortical parenchyma; RZ, rhizodermis; PC, procambium; SRC, sloughed root cap cells; VC, vascular cylinder; XP, xylem parenchima. Micrographs are representative of those obtained from 25 roots from five independent experiments. A to F, Bar = 52 μm; G and respective inset, bar = 340 μm; H, bar = 56 μm; inset in H, bar = 140 μm; I, bar = 40 μm; J, bar = 20 μm; K, bar = 16 μm.

Spd Catabolism Negatively Regulates Growth and Perturbs Cell Cycle Phase Distributions in Maize Primary Roots

To reveal whether PAO participates in root tissue differentiation, 5-d-old maize seedlings were supplied with Spd for 24 h in aerated hydroponic culture either in the presence of or in the absence of *N*-prenylagmatine (G3), a powerful and selective inhibitor of ZmPAO activity. Indeed, this compound has been shown not to affect other cell wall or plasma membrane enzymatic sources of H_2O_2, namely NADPH oxidase, peroxidase or oxalate oxidase, or proteases, such as papaine (Cona et al., 2006). To discriminate the role of the different reaction products, plants were also treated with either two H_2O_2 scavengers, *N*,*N*[1]-dimethylthiourea (DMTU) and L-ascorbic acid, or chemically synthesized ABAL, the aldehyde released during PAO-mediated Spd oxidation. Spd strongly inhibited root growth (Supplemental Table S1) by the simultaneous modulation of both cell elongation (Table I) and cell cycle phase distributions (Fig. 2). As shown in Supplemental Table S1, 1 μM Spd slightly affected root growth while 10 μM Spd was the lowest concentration at which almost complete inhibition of root total growth (94% ± 9%) was observed when compared to untreated controls, and hence this concentration was hereafter used in combined hydroponics culture treatments, such as Spd and G3, Spd and DMTU, as well as Spd and L-ascorbic acid. Put, Spm, and ABAL were supplied at a concentration equimolar to 10 μM Spd, while G3 and DMTU were used at the working concentration of 10 μM and 5 mM, respectively, as previously reported (Zacchini and De Agazio, 2001; Angelini et al., 2008). Treatment with 10 μM or 1 mM Spd resulted in a decrease in the average length of cortical parenchymal cells (Table I) without affecting PAO enzymatic activity, protein abundance (Supplemental Fig. S1), or PAO immunocytochemical localization (data not shown). Put (10 μM) did not affect root cell growth, while 10 μM Spm exerted a similar effect to 10 μM Spd (data not shown). Supply of 5 mM DMTU or 10 μM G3 partially reverted the 10 μM Spd-induced inhibition of both root growth and cortical parenchyma cell elongation (Table I), whereas 10 μM L-ascorbic acid unexpectedly inhibited root elongation, even at lower concentrations such as 1 μM, therefore being ineffective in antagonizing Spd action (Supplemental Table S2).

Furthermore, flow cytometry analysis of root tip nuclei stained with 4′,6-diamidino-2-phenylindole (DAPI) revealed that a 10 μM Spd treatment altered cell cycle phase distributions, with a reduced percentage of nuclei in S phase and a higher number of cells resting in G_1 and G_2 phases compared to untreated control (Fig. 2). Data analysis based on DNA content histograms and biparametric dot plots (forward scatter light signal/DNA) showed 36.6% and 46.8% of the cells to be in G_1 phase, 34.8% and 14.3% in S phase, and 28.6% and 38.8% in G_2 phase, for untreated and Spd-treated maize roots, respectively (Fig. 2B). Biparametric dot plots (data not shown) allowed the discrimination of true nuclei from cellular debris and aggregates, thus accounting for a more precise description of cell cycle phases. G3 and DMTU reverted Spd-induced perturbation of cell cycle phase distributions, while ABAL alone (Fig. 2) failed to affect this event, suggesting that the observed effect was exclusively induced by H_2O_2 released by PAO-mediated Spd oxidation. Both 10 μM G3 and 5 mM DMTU did not affect the proportion of cells in different phases of the

Table I. *Effect of Spd treatment on maize primary root growth and cell elongation growth of root cortical parenchyma cells*

Morphometric analysis was performed at a fixed distance (1,000 μm) from the apical meristem on eosin-stained 5-mm-long longitudinal sections of paraffin-embedded roots, from 5-d-old plants grown for 24 h in aerated hydroponics either in the absence of (control) or in the presence of Spd, G3, ABAL, and DMTU. Average root length in control: T_0, 3.0 cm; T_{24}, 6 cm. Inhibition of root growth was calculated as percentage of root length increase of untreated control. Inhibition of cell elongation growth has been calculated as percentage of total cell length of untreated control. Experiments were performed independently five times, each time measuring five roots and analyzing two sections from two different roots for each treatment. Reported results are mean values ± SD (SD was within 10% for root length). Statistical analysis was performed using ANOVA. *P* values indicate statistical significance between cell length in treated plants with respect to control plants. ns, Not significant; *P* value > 0.05; *, **, and ***, *P* values ≤ 0.05, 0.01, and 0.001, respectively. *P* values between G3/Spd and DMTU/Spd versus Spd were ≤ 0.01.

Treatment	Inhibition of Root Growth	Cell Length	Inhibition of Cell Elongation Growth
	%	μm	%
Control (untreated)	/	20.3 ± 1.6	/
G3 (10 μM)	11.0	18.9 ± 1.3 ns	6.8
ABAL (10 μM)	9.7	18.0 ± 1.3 ns	11.2
DMTU (5 mM)	8.0	19.5 ± 1.4 ns	3.9
Spd (10 μM)	94.0	11.3 ± 0.7 ***	44.3
Spd (1 mM)	100.0	7.11 ± 0.51***	65.0
G3 (10 μM) and Spd (10 μM)	49.4	16.2 ± 1.0*	20.2
DMTU (5 mM) and Spd (10 μM)	45.2	16.8 ± 1.2*	17.2

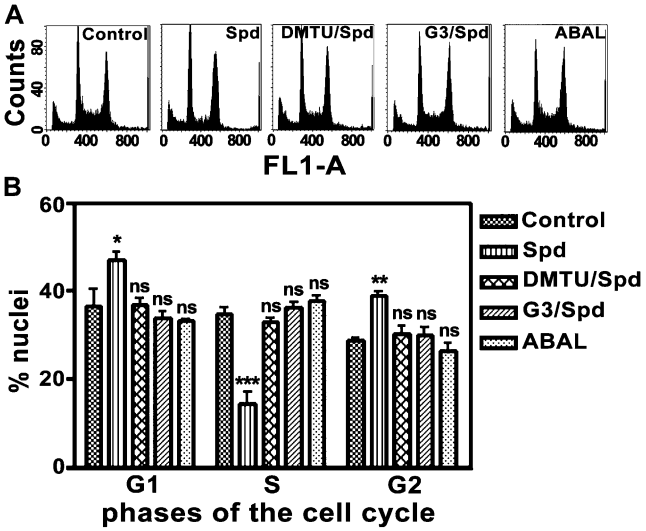

Figure 2. Effect of Spd, DMTU, G3, and ABAL exogenous supply on cell cycle phase distributions in the maize primary root tip. A, DNA fluorescence pulse area histograms of DAPI-stained nuclei isolated from maize root tips from 5-d-old plants, grown for 24 h in aerated hydroponics either in the absence of (control) or in the presence of Spd, G3, DMTU, or ABAL. FL1-A: DNA fluorescence total emission; counts: relative nuclei frequency. Cell cycle analysis were performed measuring 10^4 nuclei/sample (one typical shown for DNA fluorescence pulse area histograms). B, Data analysis based on DNA content histograms. Control: Untreated plants; Spd: 10 μM Spd-treated plants; G3/Spd: 10 μM Spd and 10 μM G3-treated plants; DMTU/Spd: 10 μM Spd and 5 mM DMTU-treated plants; ABAL: 10 μM ABAL-treated plants. Experiments were performed five times, each time utilizing 10 plants for each treatment. Results are mean values ± SD. Statistical test was performed using ANOVA. *P* values indicate statistical significance between % nuclei in each cell cycle phase in treated plants with respect to control plants. ns, Not significant; *P* value > 0.05; *, **, and ***, *P* values $\leq$ 0.05, 0.01, and 0.001, respectively.

cell cycle (data not shown). Spd at concentrations lower than 10 μM was ineffective in altering cell distribution in different phases of cell cycle, whereas higher concentrations of Spd up to 1 mM exerted a stronger effect as compared to 10 μM Spd, with a simultaneous marked increase of cellular debris and aggregates (data not shown).

Spd Induces Nuclear Condensation and DNA Fragmentation in Maize Primary Roots

To study the effect of Spd on the cell death of root tissues, paraffin-embedded transverse sections obtained at 1,000 μm from the apical meristem of the maize primary root, grown in aerated hydroponics for 24 h either in the presence of or in the absence of Spd and/or G3, DMTU, and ABAL, were analyzed using the terminal deoxynucleotidyl transferase dUTP nick end labeling (TUNEL) assay. Moreover, the analyses of nuclear dimension and chromatin condensation were carried out on digitally acquired images of nuclei stained with propidium iodide (PI; Vergani et al., 1998).

Treatment with 10 μM Spd, a concentration congruent with the corresponding level detectable in maize root tissues (Cohen, 1998) and significantly lower than that inducing PCD in tobacco leaf (0.5 mM; Takahashi et al., 2004), induced DNA fragmentation, as detected by the TUNEL in situ assay (Fig. 3C; Table II), as compared to untreated control plants (Fig. 3A; Table II), which was efficiently reverted by both G3 and DMTU (Fig. 3, E and G; Table II). DMTU or G3 alone did not induce TUNEL (Supplemental Fig. S2; Table II). Moreover, 10 μM H_2O_2 (Supplemental Fig. S2; Table II) but not ABAL (Fig. 3I; Table II), behaved as Spd in inducing TUNEL, thus indicating that Spd-induced TUNEL was exclusively mediated by H_2O_2 released via PAO-mediated Spd oxidation. Spd treatment induced chromatin condensation and reduction of nuclear volume in all tissues (Fig. 3D; Table II) as compared to untreated control plants (Fig. 3B; Table II), as also observed in Spd-treated cells of animal origin (Vergani et al., 1998), while DMTU or G3 alone did not have any effect (Supplemental Fig. S2; Table II). However, the reduction in nuclear volume and chromatin condensation were not reverted by G3 and DMTU, indicating a possible direct effect of Spd (Fig. 3, F and H; Table II), as also confirmed by the lower efficiency shown by H_2O_2 with respect to Spd in inducing nuclear condensation. DNA laddering was not observed after the aforementioned treatments (data not shown). As shown in Supplemental Figure S2 and Table II, 1 mM Spd caused a stronger effect on DNA fragmentation and chromatin condensation as compared to 10 μM Spd while 1 μM Spd failed to induce TUNEL, demonstrating that 10 μM Spd represents the lowest active concentration.

Spd Oxidation Induces Precocious Cell Death of EMX and LMX Precursors and This Hinders Full Differentiation of the Secondary Cell Wall in Maize Primary Roots

With the aim of further studying the effect of Spd on differentiation and cell death of xylem tissues, we performed electron microscopy on the apex or mature zone of maize primary roots grown in hydroponics either in the presence of or in the absence of 10 μM Spd and/or G3. Figure 4C shows that G3 treatment did not affect cytoplasm ultrastructure of cells in the apical zone at 1,000 μm from the apical meristem, as compared to untreated controls (Fig. 4A), while Spd induced apparent cytoplasm degradation (Fig. 4B), an effect that was only partly reverted by G3 (Fig. 4D). Owing to the considerable difference in total length of Spd-treated roots as compared to untreated controls, sections of mature zones were prepared from a root portion that already existed at the treatment onset, namely 1.5 cm from the seed. At this distance from the seed, EMX and LMX precursors were still alive in the untreated control roots after 24 h hydroponics, showing a well-differentiated secondary wall and regular cytoplasmic features (Fig. 4, E and I). Xylem paren-

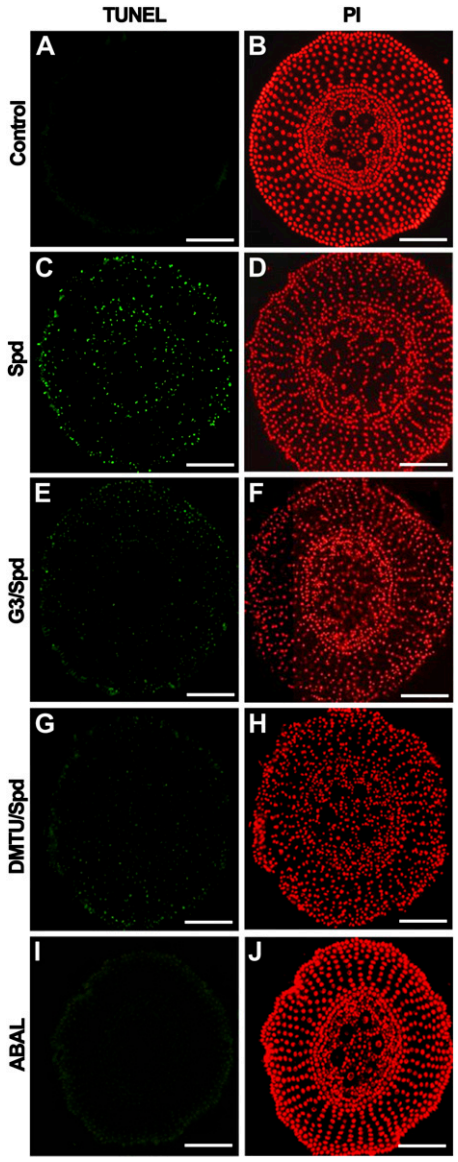

Figure 3. Effect of exogenously supplied Spd, DMTU, G3, and ABAL on DNA fragmentation detected by TUNEL in situ assay in cross sections of the maize primary root apex. A, C, E, G, and I, TUNEL staining of 10-μm-thick transversal sections at 1,000 μm from the apical meristem of paraffin-embedded maize root from 5-d-old plants, grown for 24 h in aerated hydroponics either in the absence of (control) or in the presence of Spd, G3, DMTU, or ABAL. Sections stained with PI (B, D, F, H, J) are shown for comparison. Control: Untreated plants; Spd: 10 μM Spd-treated plants; G3/Spd: 10 μM Spd and 10 μM G3-treated plants; DMTU/Spd: 10 μM Spd and 5 mM DMTU-treated plants; ABAL: 10 μM ABAL-treated plants. Micrographs are representative of those obtained from five independent experiments (the relative statistical analysis is reported in Table II). Bar = 150 μm.

chymal cells showed a very thick secondary wall and moderate cytoplasm degradation, suggestive of an initial cell death process (Fig. 4, E and I). Indeed, the walls of these cells are reported to lignify as their maturation proceeds, as assessed by floroglucinol/hydrochloric acid staining (Augeri et al., 1990). Secondary walls of xylem parenchyma and EMX cells of Spd-treated roots were very thin or even absent (Fig. 4, F and J), a condition similar to that of the same cells at the onset of the treatment (data not shown) that is likely due to early cell death of xylem precursors, a hypothesis consistent with the cytoplasmic degeneration observed in these cells.

G3 treatment also resulted in the inhibition of cell wall differentiation of both EMX and LMX elements and especially of xylem parenchymal cells (Fig. 4, G and K) as compared to control roots (Fig. 4, E and I), possibly caused by the inhibition of PAO-mediated H_2O_2 release necessary for wall maturation and as a signal for deposition of secondary wall (Potikha et al., 1999). Accordingly, an incomplete differentiation of the secondary walls of the cell types reported above was observed in specimens treated with both Spd and G3 (Fig. 4, H and L).

PAO-Mediated Spd Catabolism Induces Early Differentiation of EMX and LMX Tissues in the Maize Root Apex with Enhanced H_2O_2 Production in Xylem Tissues

Unfixed agar-embedded transverse sections obtained from the subapical zone of the primary root of maize seedlings, grown in aerated hydroponics for 24 h either in the presence of or in the absence of 10 μM Spd and/or G3, were analyzed by fluorescence microscopy under UV to visualize autofluorescence of root tissues (Fig. 5, A–D). The selection of Spd concentration was based on previous results in which PAs at concentration lower than 10 μM were ineffective in inducing TUNEL in maize roots (this work) as well as xylem differentiation in Arabidopsis roots (A. Tisi, R. Angelini, and A. Cona, unpublished data).

At 2,500 μm from the apical meristem, Spd induced a strong intensity of autofluorescence of xylem parenchyma, EMX, and LMX tissues (Fig. 5B), as compared to untreated control roots (Fig. 5A), which is indicative of the deposition of phenolics likely associated to early maturation of the cell wall and precocious cell death of xylem precursors. G3 (Fig. 5, C and D) or DMTU (data not shown) inhibited the basal levels of fluorescence, as compared to untreated control plants (Fig. 5A) as well as efficiently reverting the Spd-induced effect. H_2O_2, but not ABAL, exhibited a similar effect as compared to Spd (Supplemental Fig. S3).

A detailed analysis under laser-scanning confocal microscope (LSCM) of root serial sections allowed us to detect an intensification in phenolic autofluorescence in cell walls of xylem parenchyma as early as 200 μm from the apical meristem in Spd-treated roots (Fig. 5F) as compared to untreated control roots (Fig. 5E). Moreover, LMX and xylem parenchyma of Spd-treated roots showed increased autofluorescence especially in the intercellular spaces at approximately 1,000 μm from the apical meristem (Fig. 5, G and H) as well as in the rhizodermis outer cell wall (Fig. 5, I and J).

Table II. *Effect of Spd, G3, ABAL, DMTU, or H_2O_2 treatment on DNA fragmentation, chromatin condensation, and nuclear dimension in maize primary root, estimated by analysis of the percentage of TUNEL-positive nuclei, integrated fluorescence intensity, and nuclear diameter*

Analyses were performed after TUNEL in situ assay and PI staining of paraffin-embedded cross sections at approximately 1,000 μm from the apical meristem of maize root tissues from 5-d-old plants, grown for 24 h in aerated hydroponics either in the absence of (control) or in the presence of Spd at different concentrations, G3, ABAL, DMTU, and H_2O_2. The percentage of TUNEL-positive nuclei was calculated with respect to the number of nuclei stained with PI in the same sections. Experiments were performed independently five times, each time analyzing four sections from four different roots for each treatment (reported results are mean values; SD was within 10%). Chromatin condensation was estimated by analysis of integrated fluorescence intensity (Vergani et al., 1998). Nuclear diameter and integrated fluorescence intensity were measured using Image J software on digitally acquired images of nuclei stained with PI. Experiments were performed independently five times, each time analyzing two sections from two different roots for each treatment, by measuring 45 randomly chosen nuclei in parenchimal cells for each section (reported results are mean values ± SD). Statistical test was performed using ANOVA. *P* values indicate statistical significance between the percentage of TUNEL-positive nuclei, integrated fluorescence intensity, and nuclear diameter in treated plants with respect to control plants (rows 2–8) or with respect to 10 μM Spd (rows 9 and 10). ns, Not significant; *P* value > 0.05; *, **, and ***, *P* values ≤ 0.05, 0.01, and 0.001, respectively.

Row	Treatment	TUNEL-Positive Nuclei	Integrated Fluorescence Intensity	Nuclear Diameter
		%	$\times 10^4$	μm
1	Control (untreated)	0	1.81 ± 0.17	15.4 ± 1.5
2	G3 (10 μM)	0 ns	1.86 ± 0.18 ns	15.0 ± 1.4 ns
3	ABAL (10 μM)	0 ns	1.86 ± 0.17 ns	15.4 ± 1.5 ns
4	DMTU (5 mM)	0 ns	1.85 ± 0.18 ns	16.0 ± 1.5 ns
5	H_2O_2 (10 μM)	77.4***	1.00 ± 0.27***	10.4 ± 1.4 **
6	Spd (10 μM)	34.3***	0.75 ± 0.06***	9.0 ± 0.8***
7	Spd (1 μM)	0 ns	1.6 ± 0.14 ns	14.4 ± 1.2 ns
8	Spd (1 mM)	77.0***	0.56 ± 0.05***	9.1 ± 0.7***
9	G3 (10 μM) and Spd (10 μM)	14.4***	0.93 ± 0.10 ns	10.8 ± 1.0 ns
10	DMTU (5 mM) and Spd (10 μM)	6.4***	0.83 ± 0.07 ns	10.3 ± 0.9 ns

To get further insights into the possible effect of Spd treatment on xylem tissue differentiation we analyzed longitudinal sections stained with PI to visualize cell walls under LSCM and performed a statistical analysis of the distances between the apical meristem and the first recognizable LMX cells that showed a diameter of about 30 to 35 μm (Fig. 6B). Moreover we analyzed the distances between the apical meristem and the first EMX precursors (Fig. 6, E and F) as well as LMX cells with a diameter of about 60 to 65 μm (Fig. 6, C and D), that we used as a reference size to compare the developmental stage of LMX elements along the root length in control and Spd-treated plants. Spd induced early differentiation of the first LMX cells and the first EMX precursors with initial development of secondary walls. Indeed, in Spd-treated plants the first LMX cells with a diameter of 30 to 35 μm appeared at an average of 330 μm from the apical meristem (Fig. 6, B and G), while LMX cells showing the same size were found further than 750 μm from the apical meristem in untreated control roots (Fig. 6A), at about 900 μm (image not shown; Fig. 6G). LMX cells with 60 to 65 μm of diameter were readily recognized at approximately 500 μm from the apical meristem in Spd-treated plants (Fig. 6, D and G) while they were present only at an average of 1,400 μm in untreated control plants (Fig. 6, C and G). EMX precursors with initial development of secondary walls (Fig. 6, E and G) or extensive annular thickenings (Fig. 6F), were present in Spd-treated plants, respectively, at 1,500 and 3,000 μm from the apical meristem. In control plants they were detectable much further than 3,000 μm (image not shown; Fig. 6G).

To verify whether PAO-mediated production of H_2O_2 resulted in detectable H_2O_2 levels in xylem differentiating tissues, in situ H_2O_2 localization by in vivo DAB staining was performed in untreated control and Spd-treated maize roots. To detect the in vivo Spd-induced production of H_2O_2, DAB staining was achieved by simultaneously supplying Spd and DAB in hydroponics. As shown in Figure 6, H to J, a strong DAB staining was detectable at 1,000 μm from the apical meristem in xylem tissues of 10 μM Spd-treated primary root (Fig. 6, H and J), especially xylem parenchyma and EMX, while in untreated control roots H_2O_2 was not detected in the same zone (Fig. 6I). Notably, tissue distribution of in vivo H_2O_2 production paralleled that shown by ZmPAO hystochemical enzyme activity (Fig. 1F), further supporting the hypothesis that Spd treatment could be responsible for early xylem tissue differentiation by inducing precocious cell wall stiffening and PCD in xylem precursors via PAO-mediated H_2O_2 production. Treatment with Spd at lower concentration, such as 1 μM, induced a weaker DAB staining localized

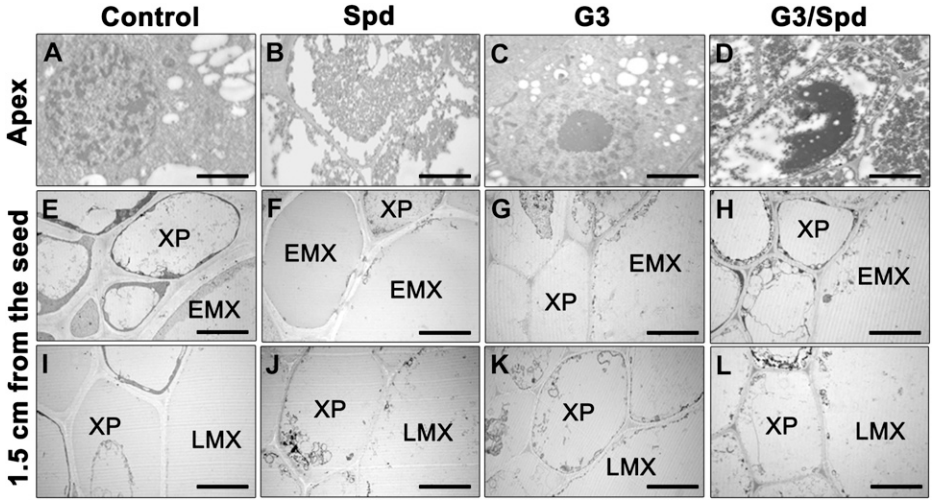

Figure 4. Effect of Spd and G3 treatment on differentiation of cortical parenchyma and xylem tissues in maize primary root. Transmission electron microscopy of cortical parenchyma cells at 1,000 μm from the apical meristem (A–D) and stelar tissues at 1.5 cm from the seed, namely a zone preexistent at the onset of treatment (E–L) of maize root from 5-d-old plants, grown for 24 h in aerated hydroponics either in the absence of (control) or in the presence of Spd and/or G3. Control: Untreated plants; Spd: 10 μM Spd-treated plants; G3: 10 μM G3-treated plants; G3/Spd: 10 μM Spd and 10 μM G3-treated plants. XP, Xylem parenchyma. Micrographs are representative fields of sections obtained from 10 roots from five independent experiments. A to D, Bar = 6 μm, magnification ×1,333; E to L, bar = 12 μm, magnification ×666.

in the outer zone of the central cylinder as compared to 10 μM Spd treatment (Supplemental Fig. S4).

Transgenic Tobacco Plants Overexpressing ZmPAO in the Apoplast Show Early Differentiation of Vascular Tissues, Increased Cell Death, and Enhanced H_2O_2 Production in Root Apices as Compared to Wild-Type Plants

To further document the fact that PAO does play a central role in tracheary element development, we analyzed xylem tissue differentiation in transgenic tobacco plants overexpressing *ZmPAO* (S-*ZmPAO*; Rea et al., 2004). These plants show a significant perturbation of ascorbate peroxidase activity indicative of altered redox state without any significant reduction in the levels of free PAs (Rea et al., 2004). Root apices from wild-type and S-*ZmPAO* tobacco plants were stained with PI to visualize cell walls under LSCM and with fluorescein diacetate-SYTOX orange double fluorescence staining, indicative of cell death. Statistical analysis (Fig. 7, C and D) demonstrated that S-*ZmPAO* exhibited early differentiation of vascular tissues (Fig. 7, B and C) and a higher level of cell death (Fig. 7, inset in B and D) as compared to wild-type plants (Fig. 7A, inset in A, C, and D). Indeed, in transgenic plants, xylem precursors with secondary wall thickening appeared at an average of 350 μm from the root cap (Fig. 7, B and E), as compared to wild-type plants where they appeared at an average of 500 μm from the root cap (Fig. 7, A and C). Moreover, a higher number of nuclei stained by SYTOX orange occurred in root cap cells and in the rhizodermis of the subapical region (up to 300 μm from the root cap) of S-*ZmPAO* tobacco plants (Fig. 7, inset in B and D) as compared to the same tissues of wild-type roots (Fig. 7, inset in A and D), with a ratio 3:1 (P value $\leq$ 0.01, the ratio was not significantly different in all Z stacks analyzed). Consistent with the results found in Spd-treated maize roots, a significantly higher generation of H_2O_2 was detected in S-*ZmPAO* tobacco roots (Fig. 7, E and F) as compared to wild-type roots (Fig. 7, G and H). In particular, H_2O_2 production was visualized by Amplex Ultra Red (AUR) staining in xylem tissue at about 370 μm from the root cap in transgenic plants (Fig. 7E), whereas in wild-type tobacco roots the first detectable H_2O_2 appeared at about 1,200 μm from the root cap (Fig. 7G). These results further support the role of H_2O_2 generated by the PAO-mediated PA oxidation in early xylem tissue differentiation and cell death.

Transgenic Tobacco Plants Down-Regulating *S*-Adenosyl-L-Met Decarboxylase Show Altered Differentiation of Vascular Tissues While Antisense *PAO* Plants Are Unaffected

To gain further insight into the role played by PAs and/or their catabolic products in xylem differentiation, transgenic tobacco plants down-regulating the gene encoding *S*-adenosyl-L-Met decarboxylase via RNAi (RNAi-*SAMDC*; Moschou et al., 2008b) or expressing the *ZmPAO* gene in the antisense orientation (A-*ZmPAO*; Moschou et al., 2008b), were examined under LSCM after PI staining.

As shown in Figure 8, RNAi-*SAMDC* plants revealed a S-*ZmPAO* plant-like phenotype, showing

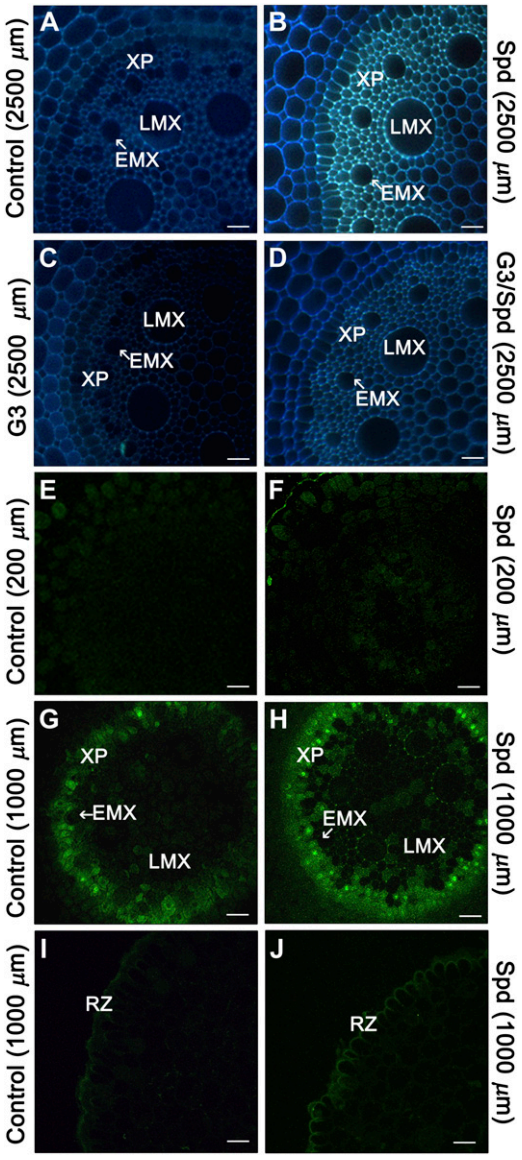

Figure 5. Effect of Spd and G3 treatment on maize primary root autofluorescence under UV and blue light. Fluorescence microscopy (A–D) and LSCM (E–J) analysis of unfixed agar-embedded maize root tissues from 5-d-old plants, grown for 24 h in aerated hydroponics either in the absence of (control) or in the presence of Spd and/or G3. A to D, UV-light-induced autofluorescence microscopy analysis of root transverse sections at 2,500 μm from the apical meristem. E to J, LSCM analysis (Z stack 3 μm, with Z-step size of 0.045 μm) of autofluorescence under blue light excitation in cross sections from maize primary root at different distances from the apical meristem (E and F: 200 μm; G to J: 1,000 μm). Control: Untreated plants; Spd: 10 μM Spd-treated plants; G3: 10 μM G3-treated plants; G3/Spd: 10 μM Spd and 10 μM G3-treated plants. RZ, Rhizodermis; XP, xylem parenchyma. Micrographs are representative of those obtained from 25 roots from five independent experiments. A to D, Bar = 20 μm; E to J, bar = 31 μm.

early differentiation of vascular tissues (Fig. 8, B and C) and increased cell death (Fig. 8, inset in B and D) as compared to wild-type plants (Fig. 8, A, C, and D). Indeed, in RNAi-*SAMDC* transgenic plants, xylem precursors appeared at an average of 380 μm from the root cap (Fig. 8, B and C), as compared to wild-type plants where they appeared at an average of 520 μm from the root cap (Fig. 8, A and C). Moreover, a higher number of nuclei stained by SYTOX orange occurred in root cap cells (up to 200 μm from the root cap) in RNAi-*SAMDC* transgenic tobacco plants (Fig. 8, inset in B and D) as compared to wild-type plants (Fig. 8, inset in A and D), with a ratio 4.4:1 (P value ≤ 0.01, the ratio was not significantly different in all Z stacks analyzed). Vascular terminal differentiation in A-*ZmPAO* plants down-regulating endogenous PAO, occurred in a similar fashion as compared to wild-type plants (not shown).

DISCUSSION

In this work we show that ZmPAO is mainly expressed in primary root tissues undergoing developmental PCD, such as EMX, LMX, and associated paratracheal parenchyma, as well as in sloughed root cap cells (Fig. 1). In xylem precursors, PAO mainly has a cytoplasmic localization and it was shown that as the cells mature, the enzyme will accumulate in the cell wall parallel to secondary wall deposition and developmental cell death (Cona et al., 2005). Development of vascular tissues is associated with cell cycle/endocycle progression and amine oxidase expression in tobacco (Paschalidis and Roubelakis-Angelakis, 2005). It has been proposed that these events are to be linked with the physiological need for the higher production of H_2O_2 via amine oxidases in the secretion pathway (Cona et al., 2005) and in the apoplast to drive peroxidase-catalyzed cross linking of cell wall polysaccharides and proteins to complete cell wall maturation, to stimulate endoreduplication, and possibly to act as a signal triggering xylem precursor cell death (Cona et al., 2005; Paschalidis and Roubelakis-Angelakis, 2005). Accordingly, Spd treatment at a concentration similar to that found in maize roots (Cohen, 1998) suppressed root growth by inhibiting cell elongation and altering cell cycle phase distributions in maize primary root apices, thus allowing cells to initiate their differentiation programs (Table I; Fig. 2). Importantly, the PAO inhibitor G3 or the H_2O_2 scavenger DMTU, reverted Spd-induced inhibition of cell growth and reduction of percentage of nuclei in S phase, while ABAL, G3, or DMTU alone failed to affect these events, thus indicating that the observed effect was exclusively mediated by H_2O_2 generated by PAO activity. Unexpectedly, the H_2O_2 scavenger L-ascorbic acid inhibited root elongation by itself, being ineffective in antagonizing Spd action (Supplemental Table S2). In fact L-ascorbic acid, although it is an effective antioxidant in vivo (Pignocchi and Foyer, 2003), is rapidly oxidized by the apoplastic ascorbate oxidase to dehydroascorbate, which can be transported into the cytoplasm to negatively affect cell cycle progression (de Pinto et al., 1999), or can be further degraded in

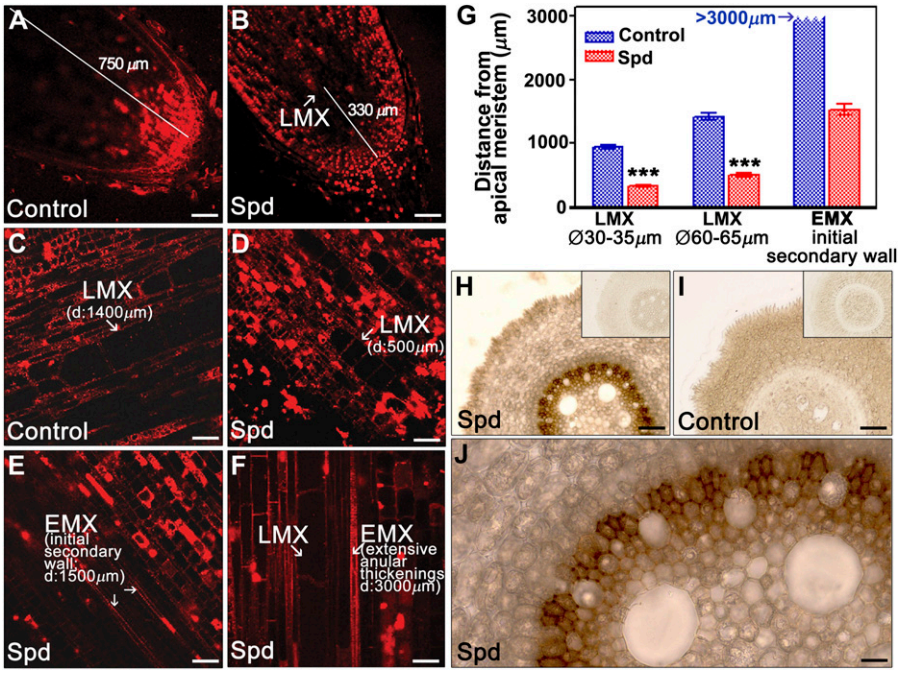

Figure 6. Effect of exogenously supplied Spd on tracheary element development and in vivo H_2O_2 production in maize primary root. PI-staining analysis under LSCM of unfixed agar-embedded longitudinal sections (A–F) and in situ DAB-staining analysis under light microscope of unfixed agar-embedded cross sections (H–J) at 1,000 μm from the apical meristem from maize primary root from 5-d-old plants, grown for 24 h in aerated hydroponics either in the absence of (control) or in the presence of 10 μM Spd. Insets in H and I illustrate cross sections without DAB supply. Control: Untreated plants; Spd: 10 μM Spd-treated plants; D, Average distance from the apical meristem. A to F, Experiments were performed five times, each time analyzing three sections from three different roots for each treatment. Micrographs are representative of those obtained. G, Distance values between xylem precursor and apical meristem were measured under LSCM exploiting the LAS AF software and then used for statistical analysis. Results are mean values ± SD. H to J, Micrographs are representative fields of sections obtained from five independent experiments, each time analyzing five roots for plant treatment. A and B, Bar = 95 μm; C to F, bar = 47.5 μm; H and I, bar = 50 μm; J, bar = 12.5 μm. *P* values have been calculated with Student's *t* test analysis, comparing distance of LMX cells from the apical meristem in Spd-treated plants with respect to untreated control plants (G). ns, Not significant; *P* value > 0.05; *, **, and ***, *P* values ≤ 0.05, 0.01, and 0.001, respectively.

the cell wall with concomitant generation of H_2O_2 (Kärkönen and Fry, 2006). Moreover, Spd treatment induced DNA fragmentation, which was also reverted by G3 or DMTU (Fig. 3). The apparent lack of DNA laddering in Spd-treated roots could be explained by the fact that this event in plants is not universal. In this regard, there is no evidence of DNA laddering in PCD of tracheary elements, in which S1-type nucleases may degrade chromosomal DNA instead of the ladder-forming nucleases seen in animal apoptosis (Ito and Fukuda, 2002). The early differentiation of xylem precursors (Figs. 4–6) associated with enhanced H_2O_2 production (Fig. 6) in Spd-treated maize primary roots, further supports the hypothesis that root differentiation could be mediated by the PAO-driven Spd oxidation. Moreover, the incomplete differentiation of the secondary wall in EMX and LMX elements observed after Spd treatment, could be interpreted as the result of a sudden H_2O_2 burst leading to premature cell death of the precursor, occurring prior to the onset of secondary wall deposition (Fig. 4). Accordingly, PAO overexpression in the cell wall of tobacco plants resulted in early differentiation of root xylem precursors and cell death of sloughed root cap cells and rhizodermis of the subapical region, as well as enhanced in vivo H_2O_2 production in xylem tissues (Fig. 7). On the other hand, the incomplete cell wall differentiation observed in these tissues after G3 treatment (Fig. 4) could be ascribed to the inhibition of PAO activity and lack of H_2O_2 production that represents an essential signal for the biosynthesis of the secondary wall (Potikha et al., 1999). Indeed, combined G3/Spd treatment resulted in an intermediate degree of differentiation of the secondary wall (Fig. 4). In apparent contradiction with our hypothesis about the role played by PA in xylem differentiation and cell death, is the finding that exogenous Spm prolongs xylem element differentiation in xylogenic *Zinnia elegans* cell cultures, reducing the time of appearance and the rate of tracheal element differentiation as well as the finding that ACL5 controls xylem specification through the prevention of premature cell death in Arabidopsis (Muñiz et al., 2008). However, this incongruity can be explained by two considerations: (1) contrary to *Z.*

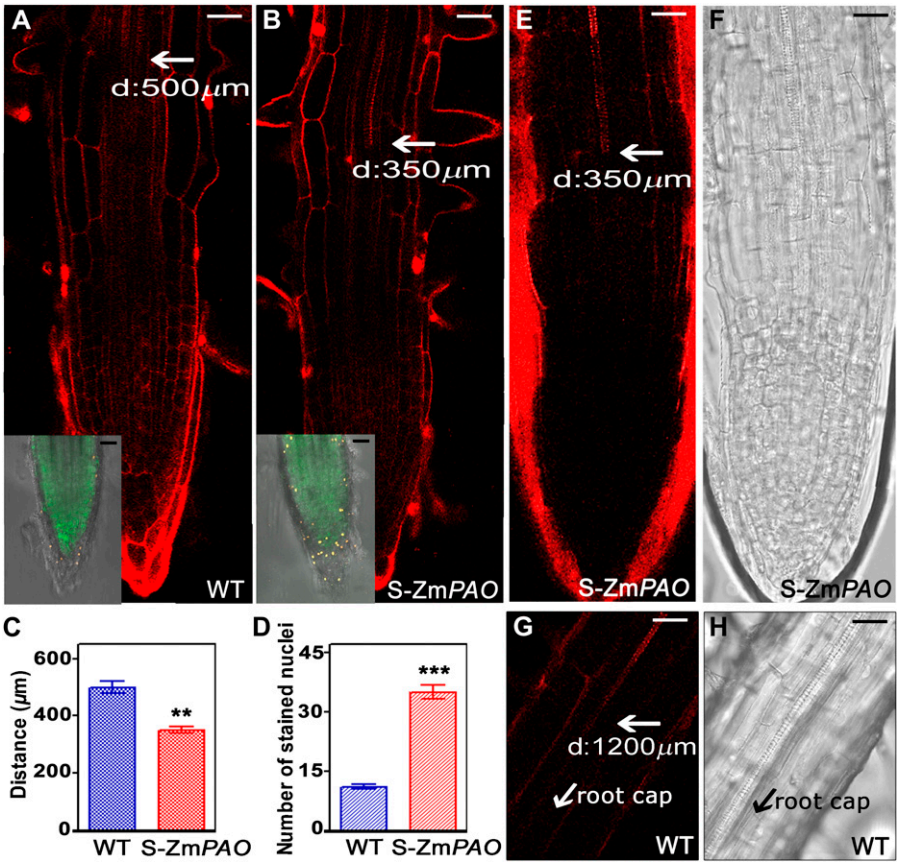

Figure 7. LSCM analysis of tracheary element development and cell death by PI (A and B) and fluorescein diacetate-SYTOX orange double fluorescence staining (inset in A and B; up to 300 μm from the root cap), respectively, and in situ H_2O_2 detection by AUR staining (E–H) in root apices of tobacco plants (cv Petit Havana SR1) both wild-type (WT) and overexpressing *ZmPAO* (S-*ZmPAO*). D, Average distance from the root cap. Micrographs are relative to the root central zone and are representative of those obtained from five independent experiments, each time analyzing five roots for plant genotype. Images in A, B, E, and F were obtained aligning multiple layers representing serial overlapping micrographs of the same root by Photoshop software. Inset in A and B represent a Z-stack analysis (thickness 20 μm with a Z-step size of 1 μm). C, Mean values ± SD relative to the distance of first xylem precursor with secondary walls from the root cap. Distance values were measured under LSCM exploiting the LAS AF software and then used for statistical analysis. D, Mean values ± SD relative to the number of nuclei stained with SYTOX orange in the central 20-μm Z stack. A and B, Inset in A and B, bar = 30 μm; E to H, bar = 30 μm. *P* values have been calculated with Student's *t* test analysis, comparing distance of xylem precursors (E) or number of SYTOX orange-labeled nuclei (F) in transgenic tobacco plants with respect to wild-type plants. ns, Not significant; *P* value > 0.05; *, **, and ***, *P* values ≤ 0.05, 0.01, and 0.001, respectively.

elegans or Arabidopsis plants, PAO expression levels are particularly high in the cytoplasm and cell wall of monocotyledons (Cohen, 1998; Cona et al., 2005) and thus the physiological role of PAs in maize root may depend on the H_2O_2 released upon PAO-mediated PA oxidation; (2) ACL5, actually being a thermospermine synthase (Knott et al., 2007), may exert its function through a specific effect of thermospermine (Kakehi et al., 2008) that is indeed a poor substrate of ZmPAO (P. Tavladoraki, personal communication).

Remarkably, down-regulation of SAMDC promoted vascular cell differentiation and induced PCD in root cap cells (Fig. 8) similarly to ZmPAO overexpression in the cell wall, suggesting that xylem differentiation and PCD induction are governed by a complex regulatory system in which intracellular PAs and apoplastic PA-derived H_2O_2 are likely integrated in coordinated signaling pathways; this is consistent with a previous hypothesis where salinity-induced cell death was proposed to be governed by the PAs/H_2O_2 ratio (Moschou et al., 2008b). In this regard, Moschou et al. (2008a, 2008b) reported that the balance between the apoplastic PA catabolism versus the intracellular PA levels plays a central role in plant responses to salinity by governing the cell fate decision, leading to either induction of PCD or to tolerance mechanisms. Specifically, it was proposed that lowering the PA anabolism/PA catabolism ratio promotes PCD (S-*ZmPAO* and RNAi-*SAMDC* plants), while if PA anabolism predominates over catabolism, PCD fails to occur, allowing simultaneous

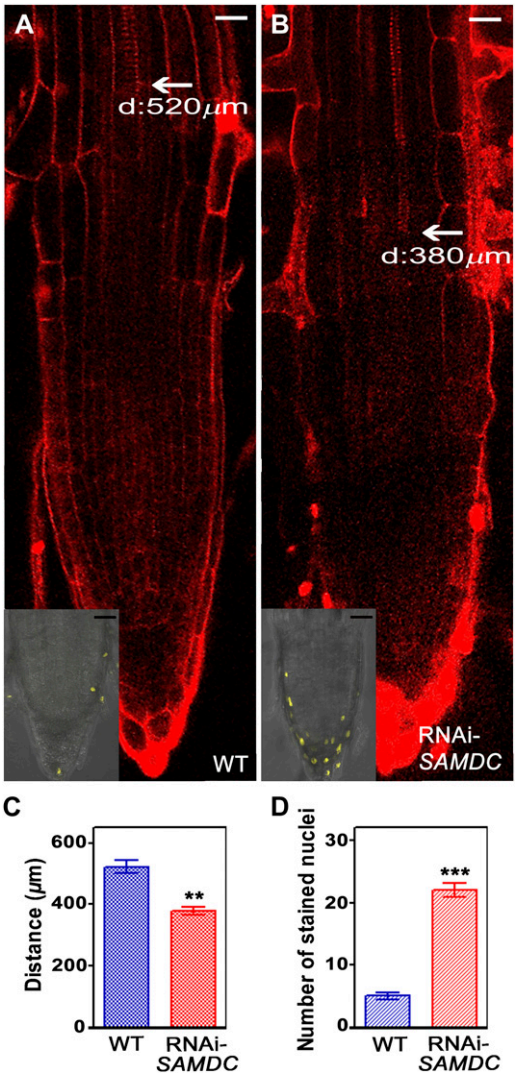

Figure 8. LSCM analysis of tracheary element development and cell death by PI (A and B) and SYTOX orange staining (inset in A and B; up to 200 μm from the root cap), respectively, in root apices of tobacco plants (cv Xanthi), both wild-type (WT) and transgenic plants down-regulating the gene encoding RNAi-*SAMDC*. Micrographs are relative to the root central zone and are representative of those obtained from five independent experiments, each time analyzing five roots per plant genotype. Images in A and B were obtained aligning multiple layers representing serial overlapping micrographs of the same root by Photoshop software. Inset in A and B represent a Z-stack analysis (thickness 20 μm with a Z-step size of 1 μm). C, Mean values ± SD relative to the distance of first xylem precursor with secondary walls from the root cap. Distance values were measured under LSCM exploiting the LAS AF software and then used for statistical analysis. D, Mean values ± SD relative to the number of nuclei stained with SYTOX orange in the central 20-μm Z stack. Bar = 25 μm. *P* values have been calculated with Student's *t* test analysis, comparing distance of xylem precursors (C) or number of SYTOX orange-labeled nuclei (D) in transgenic tobacco plants with respect to wild-type plants. ns, Not significant, *P* value > 0.05; *, **, and ***, *P* values ≤ 0.05, 0.01, and 0.001, respectively.

induction of stress-responsive genes and plant tolerance (wild-type and A-*ZmPAO* plants). Indeed, the RNAi-*SAMDC* plants, while keeping normal apoplastic Spd exodus and oxidation, exhibited constitutively lower intracellular PA levels as well as enhanced H_2O_2 production under salt stress in comparison to wild-type plants, with a PAs/H_2O_2 ratio analogous to that shown by S-*ZmPAO* plants, which also exhibited lower Spd and Spm levels and higher H_2O_2 production than the wild-type plants (Moschou et al., 2008b). In agreement with the hypothesis based on the PA/H_2O_2 ratio, our results showed that lowering the PAs/H_2O_2 ratio, by either increasing H_2O_2 production (S-*ZmPAO* transgenic plants; Fig. 7) or by decreasing PA levels (RNAi-*SAMDC* transgenic plants; Fig. 8), promoted root differentiation, resulting in a similar plant phenotype. Moreover, vascular terminal differentiation occurred in a similar fashion in A-*ZmPAO* plants down-regulating endogenous PAO (in which PA anabolism predominates over catabolism and salinity-induced PCD failed to occur; Moschou et al., 2008b) as compared to wild-type plants (not shown). Another possible explanation for the lack of phenotype shown by A-*ZmPAO* plants could be the involvement of additional and/or alternative H_2O_2 sources, such as apoplastic CuAOs, that could cooperate with PAOs in H_2O_2 delivery during tobacco xylem tissue differentiation. Indeed the simultaneous presence of CuAO and PAO activity working at the same time in the same tissues has been previously reported in tobacco, where the two enzymes have been proposed to cooperate during physiological and stress response events, such as lignification of vascular tissues (Paschalidis and Roubelakis-Angelakis, 2005) and wound healing responses (Tisi et al., 2008). Furthermore, the phenotype shown by the RNAi-*SAMDC* transgenic plants could be ascribable to the absence of some specific PA directly involved in xylem differentiation, and therefore unrelated to its catabolism to H_2O_2 and/or to the PA/H_2O_2 ratio, once more underlining the complexity of PA physiology.

Overall, the reported results obtained after Spd treatment or PAO overexpression, indicate a role for PAO in regulating differentiation and developmental cell death of xylem precursors and other root tissues, namely sloughed root cap cells. Within this context, PA biosynthesis in xylem precursors, or their secretion from neighboring paratracheal tissues, or even their phloem and xylem mediated translocation (Antognoni et al., 1998) represent a physiological source of H_2O_2 via amine oxidase activity in root stelar tissues. The abundance of PAO in xylem parenchymal cells is consistent with this concept, as it is known that this tissue may contribute to H_2O_2 supply in the xylem elements even after their autolysis (Ros Barceló, 2005). Interestingly, it has been recently highlighted that specific transcription factors involved in the modulation of the balance between cell proliferation and differentiation regulate the expression of a set of peroxidases influencing the ROS balance between the zones of cell proliferation and the

zone of cell elongation where differentiation begins (Tsukagoshi et al., 2010).

The proposed scenario is supported by several studies performed in both plants or animals, where a role of PA oxidation products in mitochondrial damage and cell death has been reported. In particular, in plants, it has been shown that PAs accumulate in the intercellular space during HR in tobacco, and that H_2O_2 produced by PAO-mediated oxidation initiates a signaling transduction pathway, mediated by mitochondrial dysfunction, leading to activation of mitogen-activated protein kinases SIPK and WIPK, up-regulation of HR-associated genes, and ultimately to cell death (Takahashi et al., 2003, 2004; Yoda et al., 2006). Other data also have emphasized the involvement of mitochondria in PCD of *Z. elegans* cells differentiating into tracheary elements (Yu et al., 2002). Even though caspases are not present in plants (Rogers, 2005; Vercammen et al., 2007), metacaspases are distant relatives of animal caspases found in protozoa, fungi, and plants (Coll et al., 2010). It has been reported that in the apoptotic process induced by hyperosmotic stress in yeast (*Saccharomyces cerevisiae*), cytochrome *c* is important for metacaspase activation, probably acting upstream of this protease in triggering cell death (Silva et al., 2005). In Arabidopsis several metacaspases control PCD (Coll et al., 2010), among which it is noteworthy to mention that metacaspase 8 is induced by H_2O_2 (He et al., 2008).

Further studies addressing the molecular mechanisms underlying these processes will be fundamental to identifying potential targets of intervention aimed at ameliorating defense responses and improving the morpho-functional traits of plants.

MATERIALS AND METHODS

Chemicals

Spd, Spm, Put, DMTU, ABAL diethyl acetal, DAB, bromelain, L-ascorbic acid, PI, fluorescein diacetate, 2-aminobenzaldehyde, DAPI, and peroxidase were from Sigma-Aldrich. AUR reagent and SYTOX orange were from Molecular Probes, Invitrogen. Ultraclear and 812 resin embedding kit were from TAAB Laboratories Equipment Ltd. Bio-Plast, Carazzi's hematoxylin, eosin Y, and eukitt were from Bio Optica. Vectabond reagent was from Vector laboratories. CNBr-activated Sepharose 4B column was from GE Healthcare. Goat anti-rabbit IgG conjugated to 5-nm colloidal gold particles, normal goat serum, and silver enhancement kit were from British Biocell Int. TUNEL, DNase1, and RNase1-DNase free were from Roche Applied Science.

G3 [*N*-(4-aminobutyl)-*N*′-(3-methyl-2-butenyl)guanidine] was prepared as previously described (Corelli et al., 2002).

ABAL was prepared by acid hydrolysis of ABAL diethyl acetal in 0.5 M HCl at room temperature. ABAL production was determined spectrophotometrically by measuring the formation of a yellow adduct ($\varepsilon_{430nm} = 1.86 \times 10^3\ M^{-1}\ cm^{-1}$) produced through the reaction of Δ^1-pyrroline with 2-aminobenzaldehyde. Assay was carried out in 0.1 M sodium phosphate buffer (pH 6.5) containing 5 mM 2-aminobenzaldehyde at 37°C. Reaction was blocked after 20 min by adding trichloroacetic acid to a final concentration of 4% (w/v).

Plant Materials and Treatments

Maize (*Zea mays* 'CORONA'; from Monsanto Agricoltura) seeds were soaked in tap water for 12 h and germinated in the dark, at 21°C over three layers of filter paper moistened with distilled water. A stock of 5-d-old maize seedlings was selected on the basis of root length (3 cm) and transferred into an aerated hydroponics culture with magnetic stirring. Seedlings were grown hydroponically for 24 h in distilled water (control plants) or alternatively supplied with Spd (ranging from 1×10^{-8} M to 1×10^{-2} M), Spm (10 μM), Put (10 μM), DMTU (5 μM), G3 (10 μM), ABAL (10 μM), H_2O_2 (10 μM), L-ascorbic acid (ranging from 1 μM to 1 mM), G3/Spd, DMTU/Spd, or L-ascorbic acid/Spd. If necessary, the pH value of the hydroponics was adjusted to 5.8. To avoid photomorphogenic effects on ZmPAO expression (Cona et al., 2003), maize seedlings were kept in the dark for the entire duration of the experiments and every technical operation was performed under photomorphogenically inactive green light. Seeds of tobacco (*Nicotiana tabacum*) both cv Petit Havana SR1 (wild-type and transgenic genotype constitutively expressing ZmPAO in the cell wall, reported as S-*ZmPAO* plants; Rea et al., 2004), and cv Xanthi (wild-type and transgenic plants expressing in the antisense orientation the *ZmPAO* gene or down-regulating the gene encoding RNAi-SAMDC, reported as A-*ZmPAO* and RNAi-*SAMDC* plants, respectively; Moschou et al., 2008b) were sown in a custom-built hydroponics culture apparatus that allows seed germination in loam and the subsequent root growth in distilled water. Tobacco plants were grown hydroponically for 3 weeks in aerated distilled water, in a growth chamber equipped with Osram Lumilux L36W/840 lamps, irradiance at plant level of approximately 150 μE $m^{-2}\ s^{-1}$, constant temperature of 24°C ± 2°C, and a 16 h day length.

Enzyme Activity, Protein Assays, and DNA Ladder Analysis

Western blot, PAO enzymatic activity, and protein level determination were carried out in maize primary root apex extracts as previously described (Angelini et al., 2008). For DNA ladder detection, genomic DNA was isolated from maize primary root apices and run on an agarose gel according to Gunawardena et al. (2001).

Autofluorescence Analysis under UV or Blue Light of Cell Wall Ester-Linked Phenolics

Cross sections (50-μm-thick) obtained with a vibratome (Vibratome Series 1000, TPI Int.) at 200, 1,000, and 2,500 μm from the apical meristem of unfixed agar-embedded segments (5-mm-long) from untreated (control) and treated maize primary roots, were collected in 0.1 M sodium phosphate buffer (pH 7.4). Sections were directly mounted on slides and observed for cell wall phenolics autofluorescence under UV light (McLusky et al., 1999) in an Axioplan 2 (Zeiss) microscope equipped with a video camera (Δ Sistemi). Digitized images were acquired by an IAS 2000 software (Δ Sistemi). Other sections were analyzed under Leica TCS-SP5 confocal microscope supplied with the Leica application suite advanced fluorescence (LAS AF) software (Leica Microsystems) using an argon laser emitting at wavelength of 488 nm and selecting the emission range from 495 to 590 nm (Angelini et al., 2008). Z stacks of 3 μm were performed with Z-step size of 0.045 μm.

Histochemical Visualization under Light Microscope of ZmPAO Enzyme Activity

Apical segments (5-mm-long) from maize primary root were fixed in 4% paraformaldehyde, 0.5% glutaraldehyde, and 0.05% Suc in 0.1 M sodium phosphate buffer (pH 6.5), for 1 h at room temperature under vacuum. After fixation, specimens were embedded in 0.4% agar. ZmPAO activity was histochemically detected in longitudinal sections using a peroxidase-coupled assay with the chromogenic peroxidase substrate DAB that is oxidized to a brown compound upon PAO-mediated H_2O_2 release after Spd supply (Augeri et al., 1990). Vibratome-cut cross sections (50-μm-thick) at different distances from the apical meristem and longitudinal sections were collected in 0.1 M sodium phosphate buffer (pH 6.5). After washing in the same buffer, longitudinal sections were preincubated in DAB-staining solution (10 mM sodium phosphate buffer [pH 6.5], containing 60 $\mu g\ mL^{-1}$ peroxidase and 0.04% [w/v] DAB) for 10 min and then incubated with 3 mM Spd in DAB-staining solution. Reactions were blocked after 3 min by thoroughly washing sections in distilled water. In cross sections, DAB staining was enhanced by addition of 0.05% (w/v) $CoCl_2$ to the staining solution, obtaining a blue color (Hsu and Soban, 1982). Sections were mounted on glass slides in 25% glycerol, prior to being observed under light microscope. Control sections incubated in the staining solution lacking Spd were negative.

Preparation of Wax-Embedded Specimen for Tissue Morphometric Analysis, ZmPAO Immunohistochemistry, and TUNEL Assay

Apical segments (5-mm-long) from untreated (control) and treated maize primary root were fixed in 2% formaldehyde, 5% acetic acid, 45% ethanol for 3 h under vacuum at 4°C. Specimens were dehydrated through a graded ethanol series (10%, 20%, 30%, 50%, 75%, 100%), 20 min each step, and then incubated overnight in 100% ethanol. Dehydrated tissues were successively taken through a graded Ultraclear series (25%, 50%, 75% in ethanol, 100%), 1 h each step, and then embedded in paraffin wax (Bio-Plast) through a graded Bio-Plast series (25%, 50%, 75% in Ultraclear, 100%), 45 min each step at 60°C. Longitudinal sections (20-μm-thick) or cross sections (10-μm-thick at approximately 1,000 μm from the apical meristem) of paraffin wax-embedded specimens were cut using a microtome (Microm HM-330; Zeiss) and collected onto slides coated with Vectabond reagent, prepared following manufacturer's instructions. Tissue sections were dewaxed in Ultraclear for 20 min and then hydrated through a graded ethanol series (100%, 95%, 90%, 80%, 70%), 5 min each step, and at the end washed in distilled water for 1 min.

Tissue Morphometric Analysis

Paraffin-embedded longitudinal sections were incubated in 1% Carazzi's hematoxylin in distilled water for 10 min, washed in distilled water for 20 min, and stained with 1% eosin Y in distilled water for 30 s. Afterward, sections were dehydrated through ethanol 95% for 1 min and ethanol 100% for 5 min and finally incubated in Ultraclear for 5 min. Sections were mounted with eukitt, prior to being observed under light microscope. Cell length was measured using Image J software (Rasband, W.S., ImageJ, U.S. National Institutes of Health, http://rsb.info.nih.gov/ij/, 1997-2008) on digitally acquired images as described above.

ZmPAO Immunohistochemistry

Paraffin-embedded cross sections were dewaxed and hydrated as described above and then processed for immunohistochemistry using a rabbit polyclonal antiserum against ZmPAO, fractionated by affinity chromatography through a CNBr-activated Sepharose 4B column coupled to bromelain, according to the manufacturer's instructions, to eliminate antiglycan antibodies (Cona et al., 2005). The resulting antiserum against ZmPAO polypeptide recognized a single protein band corresponding to ZmPAO when probed against maize crude extract. As the three maize genes encoding ZmPAO express the same protein product, the antiserum recognized all the *ZmPAO* gene products. After washing first in distilled water (30 min) and in 0.1 M sodium phosphate buffer (pH 7; buffer A) for 10 min, sections were incubated in blocking solution (5% nonfat dry milk in buffer A) for 3 h. Afterward, sections were incubated in the primary antibody diluted 1:2,000 in buffer A containing 2.5% nonfat dry milk for 24 h at 4°C. Control sections were incubated in the absence of primary antibody. Subsequently, sections were washed in buffer A (for three times 10 min each) and then incubated in goat anti-rabbit IgG conjugated to 5-nm colloidal gold particles diluted 1:200 (w/v) in medium A containing 1% normal goat serum for 2 h at room temperature. The reaction was finally visualized by using a silver enhancement kit. Anti-ZmPAO antiserum preadsorbed onto a column of CNBr-activated Sepharose 4B conjugated to pure ZmPAO (Cona et al., 2005), used as primary antibody control, and colloidal gold conjugated goat anti-rabbit IgG, used as secondary antibody control, did not show any immunoreactivity.

TUNEL Assay

The TUNEL assay was carried out on paraffin-embedded cross sections according to the manufacturer's (Roche Applied Science) instructions. Nuclei were stained by incubating in PI (2 μg/mL) for 2 min. To avoid interference due to the binding of PI to ribonucleic acids, samples were incubated in 0.5 mg/mL RNase1-DNase-free for 10 min at 37°C before starting with the TUNEL procedure. As a negative control terminal deoxynucleotidyl transferase enzyme was omitted and as a positive control, DNase1 was added, according to manufacturer's instructions (Roche Applied Science). The percentage of TUNEL-positive nuclei (excitation: 450–500 nm; emission: 515–565 nm) was calculated with respect to the number of nuclei stained with PI in the same sections (excitation: 510–530 nm; emission: 632–675 nm). Nuclear diameter and integrated fluorescence intensity for the estimation of chromatin condensation (Vergani et al., 1998) were measured using Image J software on digitally acquired images of nuclei stained with PI.

Transmission Electron Microscopy

Specimens (1-mm-long) from the apex (at about 1,000 μm from the apical meristem) or mature zone (at about 1.5 cm from the seed) of maize primary roots were fixed in 2.5% (v/v) glutaraldehyde in 0.1 M cacodylate buffer (pH 7.4), for 2 h at room temperature under vacuum aspiration. After washes in 0.1 M cacodylate buffer (pH 7.4), fragments were postfixed in 2% osmium tetroxide in 0.1 M cacodylate buffer (pH 7.4), for 2 h at 4°C, then dehydrated in graded ethanol (50%–100%) at 4°C, immersed in propylene oxide for 20 min, and gradually infiltrated with epoxy resin mixture (812 resin embedding kit), prior to embedding in the same resin. Ultrathin sections (70-nm-thick), cut from randomly chosen blocks on an ultramicrotome (Ultracut S; Leica Microsystems) were contrasted by uranyl acetate and lead citrate and collected on collodium-coated nickel grids. Sections were observed in a CM120 electron microscope (Philips) and images were electronically captured.

Flow Cytometric Analysis

Apical segments (1-cm-long) from maize primary roots (10 roots for each treatment) were thoroughly washed in cold distilled water, prior to being fixed into 30 mL formaldehyde 4% TRIS buffer (10 mM Tris/HCl, 10 mM Na_2-EDTA, 100 mM NaCl, 0.1% Triton X-100 [pH 7.5]) for 20 min at 5°C. Segments were washed three times in 30 mL Tris buffer (30 min each). Root caps (1.5–2 mm) were excised and transferred in LB01 lysis buffer (15 mM Tris/HCl, 2 mM Na_2-EDTA, 80 mM KCl, 20 mM NaCl, 0.5 mM Spm, 15 mM mercaptoethanol, 0.1% Triton X-100 [pH 7.4]; Dolezel et al., 1992). Nuclei were isolated as described by Gualberti et al. (1996) and then stained with 2 μg/mL DAPI. DAPI-stained nuclear suspensions were analyzed with a FACSVantage SE flow cytometer cell sorter (Becton Dickinson) equipped with an argon ion laser tuned to $\lambda = 351/364$ nm adjusted to 200 mW power output. Fluorescence pulse height emitted from nuclei together with integral fluorescence and width was collected through a 400-nm long-pass filter and converted on a 1,024-channel analog-to-digital converter. The instrument was aligned with chicken red blood nuclei showing a G1 DNA content histogram with a coefficient of variation better than 2.5%. VANTAGE SE amplification was adjusted so that the peak corresponding to single G1 nuclei was positioned at approximately channel 300. Flow cytometric analysis data were acquired and analyzed by the program CELLQUEST Pro v.4.01 for Mac OS (Becton Dickinson). A total of 10^4 nuclei were analyzed for each sample; all analyses were run in triplicates.

PI Staining of Cell Wall and Cell Death/Vitality Analysis

Longitudinal sections (150-μm-thick) were cut with a vibratome from agar-embedded maize primary root apices (5-mm-long) from untreated (control) and Spd-treated plants, stained with PI, and observed under LSCM at 543 nm (He-Ne laser) to reveal the outlines of cells in the root apex. The selected emission band ranged from 580 to 680 nm.

Tobacco root apices (5-mm-long), obtained from both 3-week-old tobacco cv Petit Havana SR1 plants (wild-type and transgenic S-*ZmPAO*) as well as tobacco cv Xanthi plants (wild-type, transgenic A-*ZmPAO* and transgenic RNAi-*SAMDC*), were stained with PI (10 μg/mL) in distilled water for 15 min to reveal the outlines of cells. Root apices of wild-type and transgenic S-*ZmPAO* tobacco plants (cv Petit Havana SR1) were also stained with fluorescein diacetate-SYTOX orange double fluorescence staining (5 μM SYTOX orange in distilled water for 15 min, two washes in distilled water, 10 μM fluorescein diacetate in distilled water) to discriminate between alive and dead cells. Cell death was visualized in wild type, transgenic A-*ZmPAO*, and transgenic RNAi-*SAMDC* tobacco plants (cv Xanthi) by SYTOX orange staining. Root apices stained with PI were observed under LSCM using He-Ne laser emitting at wavelength of 543 nm. The selected emission band ranged from 580 to 680 nm. Root apices stained with fluorescein diacetate-SYTOX orange double fluorescence staining were observed under LSCM (argon laser emitting at wavelength of 488 nm and He-Ne laser emitting at wavelength of 543 nm). The selected emission bands ranged from 500 to 530 nm for fluorescein diacetate and from 565 to 580 nm for SYTOX orange. Z stacks of 20 μm were performed with Z-step size of 1 μm. Shown micrographs are relative to the central Z stack.

In Situ Detection of H_2O_2 in Maize and Tobacco Root

In situ detection of H_2O_2 in the maize primary root was achieved by in vivo DAB staining (Graham and Karnovsky, 1966). Maize seedlings were grown hydroponically for 24 h in distilled water (control plants) or alternatively supplied with Spd at 10 or 1 μM. After 12 h from the beginning of the treatment, 1 μM DAB was added into the hydroponic culture of both untreated and Spd-treated plants. After further 12 h, roots were collected and sectioned for direct H_2O_2 visualization. Cross sections (50-μm-thick) obtained with a vibratome (Vibratome Series 1000, TPI Int.) at 1,000 μm from the apical meristem of unfixed agar-embedded 5-mm-long segments from untreated (control) and Spd-treated primary root, were collected in 0.1 M sodium phosphate buffer (pH 7.4). After washing, sections were directly mounted on slides and observed for DAB staining by light microscopy.

In situ detection of H_2O_2 in the tobacco root was carried out by exploiting the fluorogenic peroxidase substrate AUR that reacts in a 1:1 stoichiometry with H_2O_2 to produce a highly fluorescent reaction product (excitation/emission maxima approximately 568/581 nm). Tobacco (cv Petit Havana SR1) root apices (5-mm-long), obtained from 3-week-old wild-type and S-*ZmPAO* transgenic tobacco plants, were stained by incubation in 0.1 mM AUR, for 5 min under vacuum. After washing, root apices were observed under LSCM (HeNe laser emitting at wavelength of 543 nm). The selected emission bands ranged from 550 to 700 nm.

Statistics

Experiments were performed independently five times and a minimum of five plants for treatment were observed, unless otherwise specified, yielding reproducible results. A minimum of three sections per plant portion and treatment were examined under light and confocal microscope. Distance values between xylem precursor and apical meristem (maize plants) or root cap (tobacco plants) that have been used for statistical analysis, were measured under LSCM exploiting the LAS AF software. Five grids per block were examined in the transmission electron microscope. Single representative experiments are shown in the figures. Ten plants for each treatment were utilized in each independent experiment of flow cytometric analysis. Statistical tests were performed using GraphPad Prism with ANOVA or Student's *t* test analysis. Statistical significance of differences was evaluated by *P* level (ns, Not significant; *, **, and ***, *P* values $\leq$ 0.05, 0.01, and 0.001, respectively).

Supplemental Data

The following materials are available in the online version of this article.

Supplemental Figure S1. ZmPAO activity and protein accumulation level in the primary root apex of hydroponically grown maize plants after Spd treatment.

Supplemental Figure S2. Effect of G3, DMTU, H_2O_2, 1 μM Spd, and 1 mM Spd exogenous supply on DNA fragmentation detected by TUNEL in situ assay in cross sections of the maize primary root apex.

Supplemental Figure S3. UV light-induced autofluorescence of maize primary root after H_2O_2 or ABAL treatment.

Supplemental Figure S4. Effect of exogenously supplied Spd on in vivo H_2O_2 production in maize primary root.

Supplemental Table S1. Effect of Spd treatment on maize primary root growth, dose-response relationship.

Supplemental Table S2. Effect of L-ascorbic acid treatment on maize primary root growth.

ACKNOWLEDGMENTS

We wish to thank Paraskevi Tavladoraki for critical reading of the manuscript, Maurizio Botta for G3 preparation, and Maria Laurenzi, Martha M. Chen, and Maurizio Parenti for collaboration in experiments. Transmission electron microscopy analyses have been carried out at the Interdepartmental Laboratory of Electron Microscopy, University Roma Tre (http://www.lime.uniroma3.it).

Received January 27, 2011; accepted July 11, 2011; published July 11, 2011.

LITERATURE CITED

Angelini R, Cona A, Federico R, Fincato P, Tavladoraki P, Tisi A (2010) Plant amine oxidases "on the move": an update. Plant Physiol Biochem **48:** 560–564

Angelini R, Tisi A, Rea G, Chen MM, Botta M, Federico R, Cona A (2008) Polyamine oxidase involvement in wound-healing. Plant Physiol **146:** 162–177

Antognoni F, Fornalè S, Grimmer C, Komor E, Bagni N (1998) Long-distance translocation of polyamines in phloem and xylem of *Ricinus communis* L. plants. Planta **204:** 520–527

Augeri M, Angelini R, Federico R (1990) Sub-cellular localization and tissue distribution of polyamine oxidase in maize (*Zea mays* L.) seedlings. J Plant Physiol **136:** 690–695

Bouchereau A, Aziz A, Larher F, Martin-Tanguy J (1999) Polyamines and environmental challenges: recent development. Plant Sci **140:** 103–125

Clay NK, Nelson T (2005) Arabidopsis thickvein mutation affects vein thickness and organ vascularization, and resides in a provascular cell-specific spermine synthase involved in vein definition and in polar auxin transport. Plant Physiol **138:** 767–777

Cohen SS (1998) Plant metabolism. *In* SS Cohen, ed, A Guide to the Polyamines. Oxford University Press, Oxford, pp 396–442

Coll NS, Vercammen D, Smidler A, Clover C, Van Breusegem F, Dangl JL, Epple P (2010) *Arabidopsis* type I metacaspases control cell death. Science **330:** 1393–1397

Cona A, Cenci F, Cervelli M, Federico R, Mariottini P, Moreno S, Angelini R (2003) Polyamine oxidase, a hydrogen peroxide-producing enzyme, is up-regulated by light and down-regulated by auxin in the outer tissues of the maize mesocotyl. Plant Physiol **131:** 803–813

Cona A, Moreno S, Cenci F, Federico R, Angelini R (2005) Cellular redistribution of flavin-containing polyamine oxidase in differentiating root and mesocotyl of *Zea mays* L. seedlings. Planta **221:** 265–276

Cona A, Rea G, Angelini R, Federico R, Tavladoraki P (2006) Functions of amine oxidases in plant development and defence. Trends Plant Sci **11:** 80–88

Corelli F, Federico R, Cona A, Venturini G, Schenone S, Botta M (2002) Solution and solid-phase synthesis of aminoalkylguanidines inhibiting polyamine oxidase and nitric oxide synthase. Med Chem Res **11:** 309–321

Cuevas JC, López-Cobollo R, Alcázar R, Zarza X, Koncz C, Altabella T, Salinas J, Tiburcio AF, Ferrando A (2008) Putrescine is involved in Arabidopsis freezing tolerance and cold acclimation by regulating abscisic acid levels in response to low temperature. Plant Physiol **148:** 1094–1105

de Agazio M, Grego S, Ciofi-Luzzatto A, Rea E, Zaccaria ML, Federico R (1995) Inhibition of maize primary root elongation by spermidine: effect on cell shape and mitotic index. Plant Growth Regul **14:** 85–89

de Pinto MC, Francis D, De Gara L (1999) The redox state of the ascorbate-dehydroascorbate pair as a specific sensor of cell division in tobacco BY-2 cells. Protoplasma **209:** 90–97

Dolezel J, Cihalikova J, Lucretti S (1992) A high-yield procedure for isolation of methaphase chromosomes from root tips of *Vicia faba* L. Planta **188:** 93–98

Fincato P, Moschou PN, Spedaletti V, Tavazza R, Angelini R, Federico R, Roubelakis-Angelakis KA, Tavladoraki P (2011) Functional diversity inside the Arabidopsis polyamine oxidase gene family. J Exp Bot **62:** 1155–1168

Ge C, Cui X, Wang Y, Hu Y, Fu Z, Zhang D, Cheng Z, Li J (2006) BUD2, encoding an S-adenosylmethionine decarboxylase, is required for Arabidopsis growth and development. Cell Res **16:** 446–456

Graham RC Jr, Karnovsky MJ (1966) The early stages of absorption of injected horseradish peroxidase in the proximal tubules of mouse kidney: ultrastructural cytochemistry by a new technique. J Histochem Cytochem **14:** 291–302

Gualberti G, Dolezel J, Macas J, Lucretti S (1996) Preparation of pea (*Pisum sativum* L.) chromosomes and nuclei in suspension from single root tip. Theor Appl Genet **92:** 744–751

Gunawardena AHLAN, Pearce DM, Jackson MB, Hawes CR, Evans DE (2001) Characterisation of programmed cell death during aerenchyma formation induced by ethylene or hypoxia in roots of maize (*Zea mays* L.). Planta **212:** 205–214

He R, Drury GE, Rotari VI, Gordon A, Willer M, Farzaneh T, Woltering EJ, Gallois P (2008) Metacaspase-8 modulates programmed cell death induced by ultraviolet light and H_2O_2 in Arabidopsis. J Biol Chem **283:** 774–783

Hsu SM, Soban E (1982) Color modification of diaminobenzidine (DAB) precipitation by metallic ions and its application for double immunohistochemistry. J Histochem Cytochem **30:** 1079–1082

Imai A, Matsuyama T, Hanzawa Y, Akiyama T, Tamaoki M, Saji H, Shirano Y, Kato T, Hayashi H, Shibata D, et al (2004) Spermidine synthase genes are essential for survival of Arabidopsis. Plant Physiol **135:** 1565–1573

Ito J, Fukuda H (2002) ZEN1 is a key enzyme in the degradation of nuclear DNA during programmed cell death of tracheary elements. Plant Cell **14:** 3201–3211

Kakehi J, Kuwashiro Y, Niitsu M, Takahashi T (2008) Thermospermine is required for stem elongation in *Arabidopsis thaliana*. Plant Cell Physiol **49:** 1342–1349

Kamada-Nobusada T, Hayashi M, Fukazawa M, Sakakibara H, Nishimura M (2008) A putative peroxisomal polyamine oxidase, AtPAO4, is involved in polyamine catabolism in *Arabidopsis thaliana*. Plant Cell Physiol **49:** 1272–1282

Kärkönen A, Fry SC (2006) Effect of ascorbate and its oxidation products on H_2O_2 production in cell-suspension cultures of *Picea abies* and in the absence of cells. J Exp Bot **57:** 1633–1644

Knott JM, Römer P, Sümper M (2007) Putative spermine synthases from *Thalassiosira pseudonana* and *Arabidopsis thaliana* synthesize thermospermine rather than spermine. FEBS Lett **581:** 3081–3086

Kusano T, Berberich T, Tateda C, Takahashi Y (2008) Polyamines: essential factors for growth and survival. Planta **228:** 367–381

Kusano T, Yamaguchi K, Berberich T, Takahashi Y (2007) Advances in polyamine research in 2007. J Plant Res **120:** 345–350

Liu K, Fu H, Bei Q, Luan S (2000) Inward potassium channel in guard cells as a target for polyamine regulation of stomatal movements. Plant Physiol **124:** 1315–1326

McCully M (1995) How do real roots work? Some new views of root structure. Plant Physiol **109:** 1–6

McLusky SR, Bennett MH, Beale MH, Lewis MJ, Gaskin P, Mansfield JW (1999) Cell wall alterations and localized accumulation of feruloyl-3′-methoxytyramine in onion epidermis at sites of attempted penetration by *Botrytis allii* are associated with actin polarisation, peroxidase activity and suppression of flavonoid biosynthesis. Plant J **17:** 523–534

Medda R, Bellelli A, Pec P, Federico R, Cona A, Floris G (2009) Copper amine oxidases from plants. *In* B Mondovì, G Floris, eds, Copper Amine Oxidases: Structures, Catalytic Mechanisms and Role in Pathophysiology. CRC Press, Boca Raton, FL, pp 39–50

Møller SG, McPherson MJ (1998) Developmental expression and biochemical analysis of the Arabidopsis *atao1* gene encoding an H_2O_2-generating diamine oxidase. Plant J **13:** 781–791

Moschou PN, Delis ID, Paschalidis KA, Roubelakis-Angelakis KA (2008a) Transgenic tobacco plants overexpressing polyamine oxidase are not able to cope with oxidative burst generated by abiotic factors. Physiol Plant **133:** 140–156

Moschou PN, Paschalidis KA, Delis ID, Andriopoulou AH, Lagiotis GD, Yakoumakis DI, Roubelakis-Angelakis KA (2008b) Spermidine exodus and oxidation in the apoplast induced by abiotic stress is responsible for H_2O_2 signatures that direct tolerance responses in tobacco. Plant Cell **20:** 1708–1724

Moschou PN, Sanmartin M, Andriopoulou AH, Rojo E, Sanchez-Serrano JJ, Roubelakis-Angelakis KA (2008c) Bridging the gap between plant and mammalian polyamine catabolism: a novel peroxisomal polyamine oxidase responsible for a full back-conversion pathway in Arabidopsis. Plant Physiol **147:** 1845–1857

Moschou PN, Sarris PF, Skandalis N, Andriopoulou AH, Paschalidis KA, Panopoulos NJ, Roubelakis-Angelakis KA (2009) Engineered polyamine catabolism preinduces tolerance of tobacco to bacteria and oomycetes. Plant Physiol **149:** 1970–1981

Muñiz L, Minguet EG, Singh SK, Pesquet E, Vera-Sirera F, Moreau-Courtois CL, Carbonell J, Blázquez MA, Tuominen H (2008) ACAULIS5 controls Arabidopsis xylem specification through the prevention of premature cell death. Development **135:** 2573–2582

Paschalidis KA, Roubelakis-Angelakis KA (2005) Sites and regulation of polyamine catabolism in the tobacco plant: correlations with cell division/expansion, cell cycle progression, and vascular development. Plant Physiol **138:** 2174–2184

Pignocchi C, Foyer CH (2003) Apoplastic ascorbate metabolism and its role in the regulation of cell signalling. Curr Opin Plant Biol **6:** 379–389

Potikha TS, Collins CC, Johnson DI, Delmer DP, Levine A (1999) The involvement of hydrogen peroxide in the differentiation of secondary walls in cotton fibers. Plant Physiol **119:** 849–858

Rea G, de Pinto MC, Tavazza R, Biondi S, Gobbi V, Ferrante P, De Gara L, Federico R, Angelini R, Tavladoraki P (2004) Ectopic expression of maize polyamine oxidase and pea copper amine oxidase in the cell wall of tobacco plants. Plant Physiol **134:** 1414–1426

Rogers HJ (2005) Cell death and organ development in plants. Curr Top Dev Biol **71:** 225–261

Ros Barceló A (2005) Xylem parenchyma cells deliver the H_2O_2 necessary for lignification in differentiating xylem vessels. Planta **220:** 747–756

Seiler N, Raul F (2005) Polyamines and apoptosis. J Cell Mol Med **9:** 623–642

Silva RD, Sotoca R, Johansson B, Ludovico P, Sansonetty F, Silva MT, Peinado JM, Côrte-Real M (2005) Hyperosmotic stress induces metacaspase- and mitochondria-dependent apoptosis in *Saccharomyces cerevisiae*. Mol Microbiol **58:** 824–834

Stefanelli C, Bonavita F, Stanic′ I, Mignani M, Facchini A, Pignatti C, Flamigni F, Caldarera CM (1998) Spermine causes caspase activation in leukaemia cells. FEBS Lett **437:** 233–236

Stefanelli C, Stanic′ I, Zini M, Bonavita F, Flamigni F, Zambonin L, Landi L, Pignatti C, Guarnieri C, Caldarera CM (2000) Polyamines directly induce release of cytochrome c from heart mitochondria. Biochem J **347:** 875–880

Takahashi Y, Berberich T, Miyazaki A, Seo S, Ohashi Y, Kusano T (2003) Spermine signalling in tobacco: activation of mitogen-activated protein kinases by spermine is mediated through mitochondrial dysfunction. Plant J **36:** 820–829

Takahashi Y, Uehara Y, Berberich T, Ito A, Saitoh H, Miyazaki A, Terauchi R, Kusano T (2004) A subset of hypersensitive response marker genes, including *HSR203J*, is the downstream target of a spermine signal transduction pathway in tobacco. Plant J **40:** 586–595

Tavladoraki P, Rossi MN, Saccuti G, Perez-Amador MA, Polticelli F, Angelini R, Federico R (2006) Heterologous expression and biochemical characterization of a polyamine oxidase from Arabidopsis involved in polyamine back conversion. Plant Physiol **141:** 1519–1532

Tisi A, Angelini R, Cona A (2008) Wound healing in plants: cooperation of copper amine oxidase and flavin-containing polyamine oxidase. Plant Signal Behav **3:** 204–206

Torrigiani P, Serafini-Fracassini D, Bagni N (1987) Polyamine biosynthesis and effect of dicyclohexylamine during the cell cycle of *Helianthus tuberosus* tuber. Plant Physiol **84:** 148–152

Tsukagoshi H, Busch W, Benfey PN (2010) Transcriptional regulation of ROS controls transition from proliferation to differentiation in the root. Cell **143:** 606–616

Urano K, Hobo T, Shinozaki K (2005) Arabidopsis ADC genes involved in polyamine biosynthesis are essential for seed development. FEBS Lett **579:** 1557–1564

Vera-Sirera F, Minguet EG, Singh SK, Ljung K, Tuominen H, Blázquez MA, Carbonell J (2010) Role of polyamines in plant vascular development. Plant Physiol Biochem **48:** 534–539

Vercammen D, Declercq W, Vandenabeele P, Van Breusegem F (2007) Are metacaspases caspases? J Cell Biol **179:** 375–380

Vergani L, Mascetti G, Nicolini C (1998) Effects of polyamines on higher-order folding of *in situ* chromatin. Mol Biol Rep **25:** 237–244

Wallace HM, Fraser AV, Hughes A (2003) A perspective of polyamine metabolism. Biochem J **376:** 1–14

Walters DR (2003) Polyamines and plant disease. Phytochemistry **64:** 97–107

Wang X, Ikeguchi Y, McCloskey DE, Nelson P, Pegg AE (2004) Spermine synthesis is required for normal viability, growth, and fertility in the mouse. J Biol Chem **279:** 51370–51375

Wu J, Shang Z, Wu J, Jiang X, Moschou PN, Sun W, Roubelakis-Angelakis KA, Zhang S (2010) Spermidine oxidase-derived HO regulates pollen plasma membrane hyperpolarization-activated Ca(2+)-permeable channels and pollen tube growth. Plant J **63:** 1042–1053

Yoda H, Hiroi Y, Sano H (2006) Polyamine oxidase is one of the key elements for oxidative burst to induce programmed cell death in tobacco cultured cells. Plant Physiol **142:** 193–206

Yu X-H, Perdue TD, Heimer YM, Jones AM (2002) Mitochondrial involvement in tracheary element programmed cell death. Cell Death Differ **9:** 189–198

Zacchini M, De Agazio M (2001) Dimethylthiourea, a hydrogen peroxide trap, partially prevents stress effects and ascorbate peroxidase increase in spermidine-treated maize roots. Plant Cell Environ **24:** 237–244

Zhao F, Song C-P, He J, Zhu H (2007) Polyamines improve K^+/Na^+ homeostasis in barley seedlings by regulating root ion channel activities. Plant Physiol **145:** 1061–1072